Organic Frameworks

DOI: 10.1002/anie.201005919

Synthesis of Metallophthalocyanine Covalent Organic Frameworks That Exhibit High Carrier Mobility and Photoconductivity**

*Xuesong Ding, Jia Guo, Xiao Feng, Yoshihito Honsho, Jingdong Guo, Shu Seki, Phornphimon Maitarad, Akinori Saeki, Shigeru Nagase, and Donglin Jiang**

Covalent organic frameworks (COFs) are a new class of porous architectures that allow the integration of organic units with atomic precision into long-range-ordered two- and three-dimensional structures.[1,2] From a synthetic point of view, COFs are intriguing as they allow a new degree of control of porosity, composition, and component positions.[1–6] As high-surface-area materials that link elements of low atomic mass by covalent bonds, COFs exhibit considerable potential for gas adsorption applications. As the first report on COFs in 2005,[1a] several families of COFs have been reported.[1–6] However, the construction of COFs has to date been limited to certain monomers, and the lack of suitable procedures that utilize other units has impeded further advances in this emerging field. To advance this field it is therefore important to extend the limited number of synthetic methods and monomer units available.

Phthalocyanines are large, planar π-electronic macrocycles with broad absorption profiles that could serve as intriguing units in the construction of porous frameworks.[7,8] Crystalline phthalocyanine metal–organic frameworks have been shown to be useful in applications such as gas adsorption owing to their extended porous structures.[7] However, phthalocyanine-based porous covalent polymers are usually amorphous and disordered.[8] The combination of phthalocyanine units into a well-defined covalent framework thus remains an undeveloped area of research, offering great potential for obtaining novel functionality depending on the particular alignment and stacking.[6] The eclipsed stacking endows arene-based COFs with unique functionality, such as excimer emission, exciton migration, and photoresponse.[4] Herein, we have developed a new phthalocyanine unit for the synthesis of nickel phthalocyanine-based COFs (NiPc COF; Scheme 1). The compound, based on (2,3,9,10,16,17,23,24-octahydroxyphthalocyaninato)nickel(II), [$(OH)_8$PcNi], which has four catechol pairs at peripheral phenyl rings of a phthalocyanine macrocycle. These 2D COFs provide pre-organized conduction paths based on precise ordering of the phthalocyanine stack and are ideal for charge carrier transport. Herein we present the high-throughput synthesis and unique properties of the two-dimensional metallophthalocyanine-based COF.

The NiPc COF was synthesized by the boronate esterification reaction of [$(OH)_8$PcNi] and 1,4-benzenediboronic acid (BDBA) in dimethylacetamide (DMAc)/*o*-dichlorobenzene under solvothermal conditions (Scheme 1a). [$(OH)_8$PcNi] has low solubility in common organic solvents owing to its large π system and highly planar structure; typical procedures for the esterification reaction does not lead to the formation of desirable crystalline COFs. With reference to a well-established solvent combination (mesitylene/dioxane) for the synthesis of boronate-linked 2D COFs,[1,2,4] we investigated the reaction using different pairs of aromatic solvents (mesitylene, toluene, and *o*-dichlorobenzene) with hydrophilic solvents (dioxane, dimethylformamide (DMF), and dimethylacetamide (DMAc)). Combinations and results for the esterification reaction are summarized in the Supporting Information, Figure S1. The optimal combination for the preparation of the COFs was found to be *o*-dichlorobenzene and DMAc. Furthermore, the ratio of *o*-dichlorobenzene to DMAc was varied from 1:1 to 1:9 (vol/vol) to investigate the effect on crystallinity, as monitored by powder X-ray diffraction (PXRD) measurements. A mixture of *o*-dichlorobenzene/DMAc (1:2 vol/vol) gave the best result, as indicated by the intensity of the PXRD signals (Supporting Information, Figure S1). The NiPc COF was synthesized as a dark green powder in 90% yield. It is notable that this method gives a yield that is much higher than the previously reported value (48%).[6]

Fourier-transform infrared (FTIR) spectra of the NiPc COF exhibited characteristic bands that are due to the boronate ester at 1053, 1089, 1291, and 1347 cm^{-1}, and a typical C=N stretch at 1480 cm^{-1} for the phthalocyanine units (Supporting Information, Figure S2, Table S1). Solid-state ^1H–^{13}C CP/MAS NMR spectroscopy using a 920 MHz ^1H NMR spectrometer at a MAS rate of 15 kHz and a

[*] X. Ding,[+] Dr. J. Guo,[+] X. Feng, Dr. P. Maitarad, Prof. Dr. D. Jiang
Department of Materials Molecular Science
Institute for Molecular Science
5-1 Higashiyama, Myodaiji, Okazaki 444-8787 (Japan)
Fax: (+81) 564-59-5520
E-mail: jiang@ims.ac.jp
Prof. Dr. D. Jiang
Precursory Research for Embryonic Science and Technology (PRESTO) Japan Science and Technology Agency (JST)
Chiyoda-ku, Tokyo 102-0075 (Japan)
Y. Honsho, Prof. Dr. S. Seki, A. Saeki
Department of Applied Chemistry, Graduate School of Engineering
Osaka University, 2-1 Yamadaoka, Suita, Osaka 565-0871 (Japan)
Dr. J. Guo, Prof. Dr. S. Nagase
Department of Theoretical and Computational Molecular Science
Institute for Molecular Science
38 Nishigo-naka, Myodaiji, Okazaki 444-8585 (Japan)
[+] These authors contributed equally to this work.

[**] This work is supported by Precursory Research for Embryonic Science and Technology (PRESTO) (Japan) Science and Technology Agency (JST) (D.J.).

Supporting information for this article is available on the WWW under http://dx.doi.org/10.1002/anie.201005919.

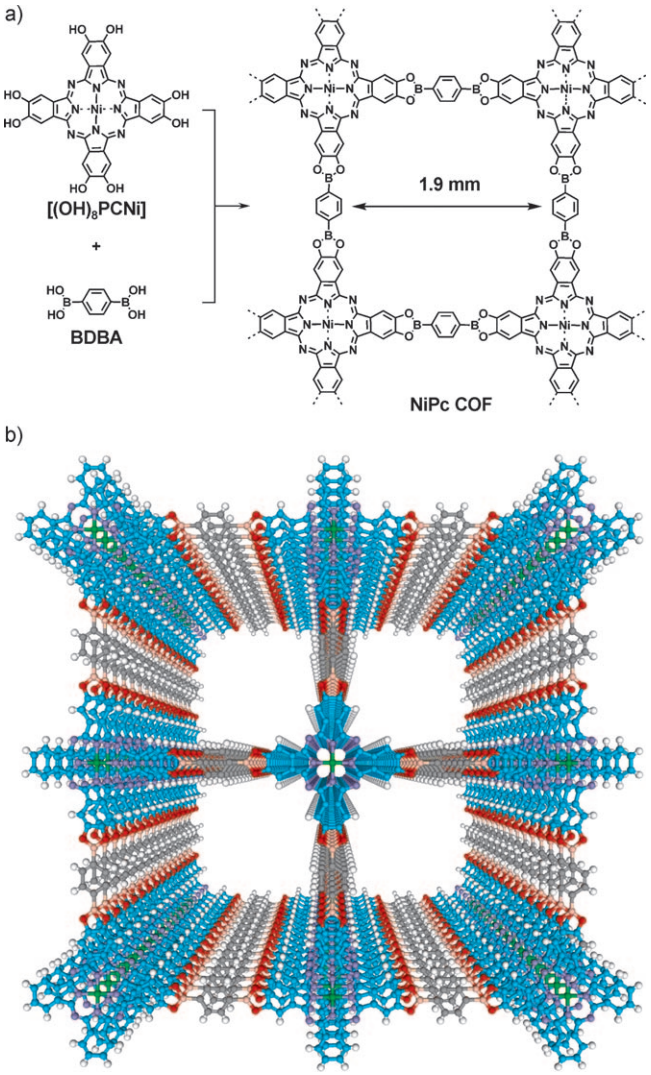

Scheme 1. a) The synthesis of the nickel phthalocyanine covalent organic framework (NiPc COF) by a boronate esterification reaction. b) Eclipsed stack of phthalocyanine 2D sheets and microporous channels in NiPc COF (a 2×2 grid is shown). Colors used for identification: phthalocyanine unit: sky blue; Ni green, N violet, C gray, O red, B orange, H white.

cross-polarization contact time of 2 ms gave three signals at $\delta = 148.52$, 130.12, and 103.14 ppm, which can be assigned to carbon atoms of the phthalocyanine and phenyl groups, respectively (Supporting Information, Figure S3). Elemental analyses confirmed that the contents of C, H, N, and Ni were 52.70, 2.91, 11.72, and 6.55, respectively, which were close to the theoretical values of 59.60, 1.80, 12.64, and 6.62 expected for an infinite sheet. The deviation in C content is slightly smaller than that reported for the free-base phthalocyanine COFs(10% deviation).[6] Field-emission scanning electron microscopy (FE-SEM) revealed that the NiPc COF adopted a layered sheet structure (Figure 1), with the size of the sheets highly dependent on the reaction temperature and duration; increasing the reaction temperature or duration led to the formation of large sheets in general (Supporting Information, Figure S4). For example, samples prepared at 120°C over

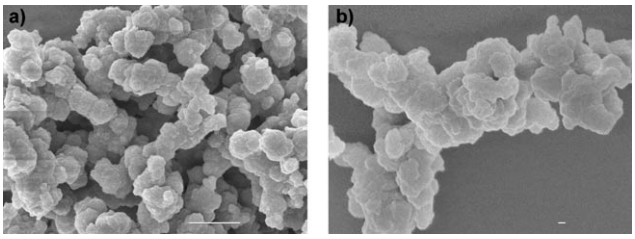

Figure 1. a) Field-emission microscopic image of a typical NiPc COF sample (scale bar: 1 μm). b) Image of NiPc COF objects at higher magnification (scale bar: 100 nm).

three days gave small sheets on the scale of several tens of nanometers, whereas those prepared at 160°C over 21 days increased to several hundred nanometers on average. The PXRD intensities and patterns of the as-prepared NiPc COFs were almost identical. High-resolution transmission electron microscopy (HR-TEM) measurements of the NiPc COF indicated a layered structure of parallel 2D sheets with an average separation of 3.3 Å (Supporting Information, Figure S5). Certain domains were observed to have tetragonal textures, and the center-to-center distance between neighboring pores was estimated to be 2.3 nm (Supporting Information, Figure S5).

PXRD patterns of the NiPc COF exhibited strong diffraction peaks at 3.78°, 7.72°, 11.56°, and 26.62° assignable to 100, 200, 300, and 001 facets, respectively (Figure 2a, red curve). Based on the PXRD pattern, the center-to-center distance between neighboring pores was evaluated to be 2.36 nm and the separation between the sheets as 3.32 Å. To elucidate the layer structure, we first carried out semi-empirical calculations at PM3 level and then performed with hybrid density functional theory (DFT) at the B3LYP level, using a double-zeta basis set (Lanl2dz) with the effective core potential (Lanl2 ECP) for Ni atoms, and the

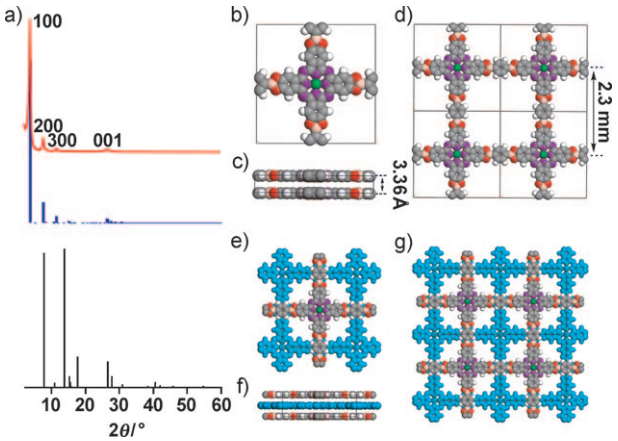

Figure 2. a) Powder X-ray diffraction profile of NiPc COF (red curve), and simulated PXRD patterns using the *P4/mmm* (blue curve) and *I4* (black curve) space groups. b–d) Views of the unit cell derived from the *P4/mmm* space group along b) *z* and c) *y* axes, and d) the structure of a single pore. e–g) Views of the unit cell of the *I4* space group along e) *z* and f) *y* axes, and g) the structure of a staggered 2×2 pore.

3-21G basis set for all other atoms using the Gaussian 03 program. The tetragonal pore unit had a planar structure (Supporting Information, Figure S6). Pawley refinements were performed to determine the final lattice parameters using Reflex (implemented in Materials Studio version 4.4), a software package for crystal structure determination based on the PXRD pattern. Simulations using the *P*4/*mmm* space group with $a = b = 23.12247$ Å and $c = 3.36358$ Å gave a PXRD pattern that was in good agreement with the experimentally observed pattern (Figure 2a). Figure 2b and c showed the derived unit-cell structure. In this formulation, the phthalocyanine units are located at nodes separated by 2.3 nm in the 2D plane (Figure 2d) and stack to form layers separated by a distance of 3.36 Å (Figure 2c). In contrast, the staggered arrangement of layers resulting from an *I*4 space group did not reproduce the experimental PXRD pattern at all (Figure 2a, black curve). Figure 2e and f show the unit cell of the *I*4 space group in a staggered stacking arrangement. In this arrangement, the phthalocyanine units overlap on the pores of the neighboring plane (Figure 2g).

The crystalline structure observed for the prepared sample after desolvation thus shows that there are open micropores of 1.9 nm in width. To evaluate the porous structure, nitrogen sorption isotherm measurements were carried out. Reversible sorption profiles were observed with typical type I sorption characteristics (Figure 3a). The Brunauer–Emmett–Teller (BET) surface area and pore volume were calculated to be as high as 624 $m^2 g^{-1}$ and 0.4854 $cm^3 g^{-1}$, respectively. The pore size calculated with the nonlocal density functional theory (NLDFT) method was nearly 1.9 nm (Figure 3b). The pore-size distribution profile confirmed that the intrinsic porosity mainly originated from the tetragonal cells (Figure 3b). All of the above results indicate that the NiPc COF is a crystalline material with well-organized stacking of the phthalocyanine units.

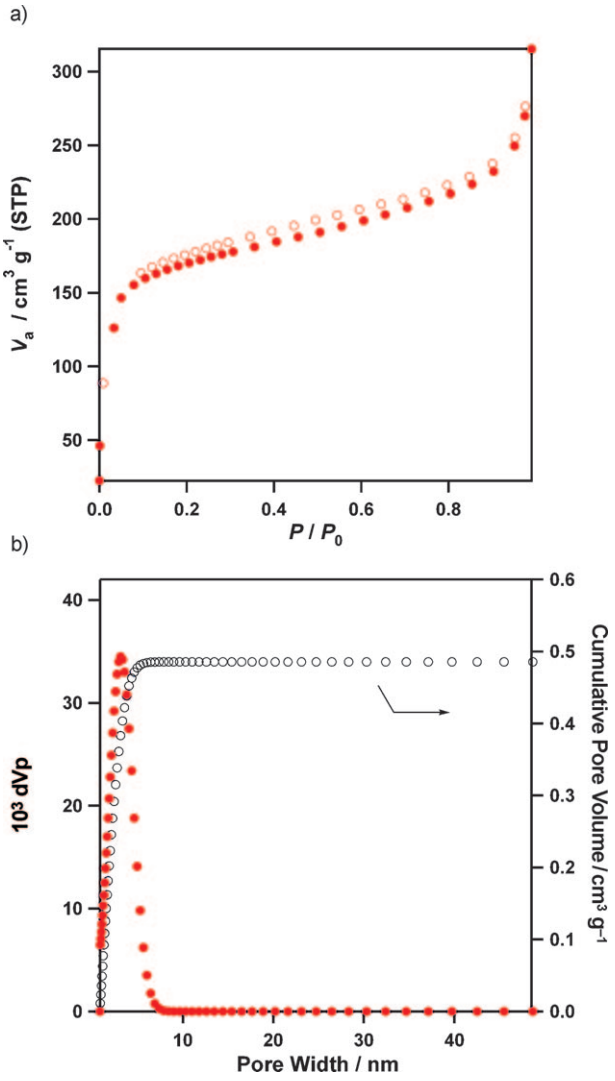

Figure 3. a) Nitrogen sorption isotherm curve measured at 77 K. b) Pore-size (red, left axis) and pore-size distribution profiles (black, right axis).

In the absorption spectra, the NiPc COF exhibited an absorption band at 380 nm that is due to the B band, which was blue-shifted by 32 nm from that (412 nm) of the monomer precursor [$(MeO)_8$PcNi] (Figure 4a). This significant blue shift indicates the formation of H-aggregates of phthalocyanine units in the stacked structure, which is in good agreement with the PXRD results. On the other hand, the Q bands of the NiPc COF were observed at 635 and 686 nm, which were red-shifted by 12 nm from those (622 and 674 nm) of [$(MeO)_8$PcNi]. Interestingly, the NiPc COF showed much greater absorption of deep-red visible and near-infrared photons than [$(MeO)_8$PcNi]. The relative intensity ratio of the Q band to the B band was 2.6 for the NiPc COF, in sharp contrast to the value of 1.3 for [$(MeO)_8$PcNi]. These results indicate that the construction of 2D COFs with stacked phthalocyanine structures enhanced their absorption capability in the long-wavelength visible and near-infrared regions.

In conductivity experiments, the NiPc COF was shown to be semiconducting, exhibiting a linear *I*–*V* curve when sandwiched between Au and Al electrodes (Figure 4b, red curve). In contrast, [$(MeO)_8$PcNi] showed a very low current under identical conditions (Figure 4b, black curve). The intrinsic charge-carrier mobility of the NiPc COF was measured by laser flash-photolysis time-resolved microwave conductivity measurements (FP-TRMC).[9,10] To evaluate the exciton–exciton annihilation effect on the carrier generation, experiments with lasers at different photon densities, from 4.5×10^{14} to 1.5×10^{16} photons cm^{-2}, were carried out (Figure 4c). The $\phi\Sigma\mu$ values ($\Sigma\mu$ = the sum of carrier mobility, ϕ = the charge carrier generation efficiency) decreased and reach constant at 3.9×10^{-5} $cm^2 V^{-1} s^{-1}$ when the photon density decreased to 6.5×10^{14} photon cm^{-2}. This observation indicates that the free charge carriers are generated by single photon processes via the NiPc COF excited states. To determine the number of charge carriers, the time-of-flight transient was integrated at different bias voltages at a photon density of 6.5×10^{14} photon cm^{-2} (Figure 4d). The number of charge carriers estimated by extrapolation of the bias at 0 V was 3.8×10^8, leading to a charge carrier generation efficiency ϕ of 3.0×10^{-5}. Changing the atmosphere of the measurements did not affect the above results, which indicates that the carrier species originates predominately from holes. The

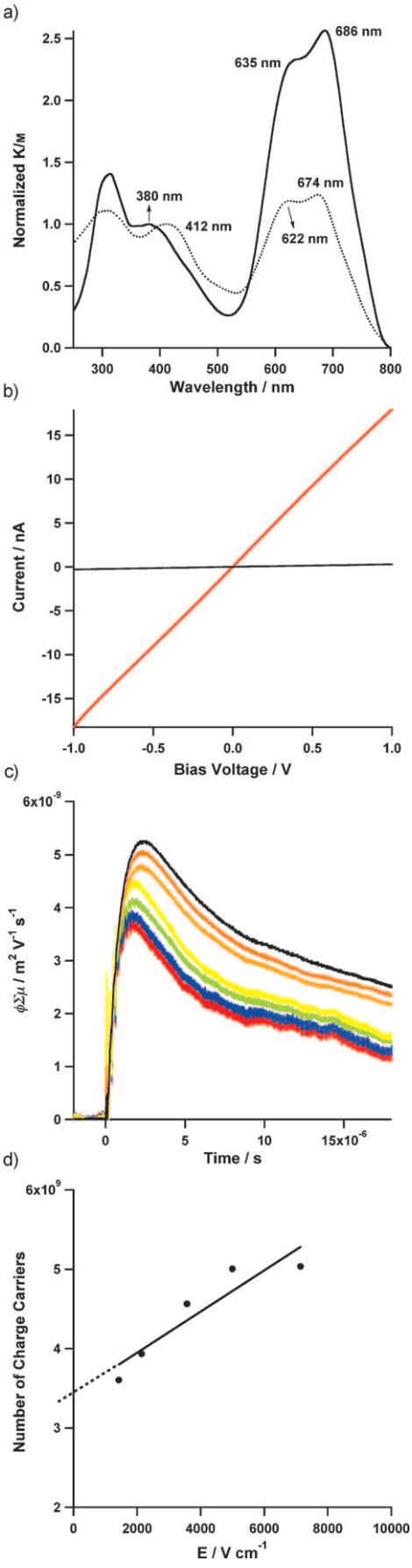

minimum mobility (μ^+) was thus evaluated to be as high as 1.3 $cm^2 V^{-1} s^{-1}$. This intrinsic carrier mobility is much higher than those of typical one- and three-dimensional conjugated polymers.[9,10]

Owing to ordered stacking of the phthalocyanine units, the NiPc COF becomes photoconductive, generating a prominent photocurrent. Irradiation from a xenon light source (>400 nm) with a UV cut-off module resulted in a significant increase in current from 20 nA (dark current) to 3 μA (photocurrent) (Figure 5a). Further, on–off switching experiments showed that the NiPc COF quickly responded to light irradiation and that the photocurrent can be switched on and off many times without deterioration (Figure 5b, red curve). In contrast, [$(MeO)_8$PcNi] did not show any photoresponse under the same conditions (Figure 5b, black curve). To investigate the wavelength dependence of the photosensitivity, we irradiated with light passed through band-path filters (±5 nm). As shown in Figure 5c, the NiPc COF was panchromatically responsive to different wavelengths and was extremely sensitive to deep-red and near-infrared photons. The increased light-harvesting capability and enhanced carrier mobility accounts for the high photoconductivity and sensitivity.

As demonstrated above, the metallophthalocyanine 2D COFs provide a unique way to align the large π-system macrocycles into the ideal stacking order for charge carrier transportation and triggering photochemical events. Such molecular alignment is not accessible with conventional polymeric approaches and hardly achieved by supramolecular architectures. Moreover, the porous channels of 2D COFs make it possible to further modulate COF properties by filling the well-defined nanospaces with counterpart molecules.

In summary, we have developed a procedure for the integration of large metallophthalocyanine π-systems into two-dimensional covalent organic frameworks based on a boronate esterification reaction using octahydroxyphthalocyanine and phenylene diboronic acid as building units in 90% yield of isolated product. The resulting NiPc COF material consists of a layered structure of planar sheets, with uniform microporous channels and a large resulting surface area. Owing to well-ordered stacking of the phthalocyanine unit, the NiPc COF shows enhanced light-harvesting capability in the visible and near-infrared regions, is semiconducting, and facilitates charge carrier transport. As a result, the NiPc COF is highly photoconductive, exhibiting a panchromatic light response and exceptional sensitivity to visible and near-infrared photons. These properties are unique and highly correlated with the structure of the NiPc COF. The remarkable results presented herein demonstrate the enormous

Figure 4. a) Absorption profiles of NiPc COF (——) and [$(MeO)_8$PcNi] (•••••). b) *I–V* curves of NiPc COF (red curve) and [$(MeO)_8$PcNi] (black curve) sandwiched between Al/Au electrodes. c) Transient conductivity profiles upon irradiation with a 355 nm pulsed laser at different photon densities: 4.5×10^{14} (red curve) to 1.5×10^{16} photon cm^{-2} (black curve). d) Number of charge carriers measured by the time-of-flight transient current integration at different bias voltages, irradiated with a 355 nm pulsed laser at 6.5×10^{14} photon cm^{-2}.

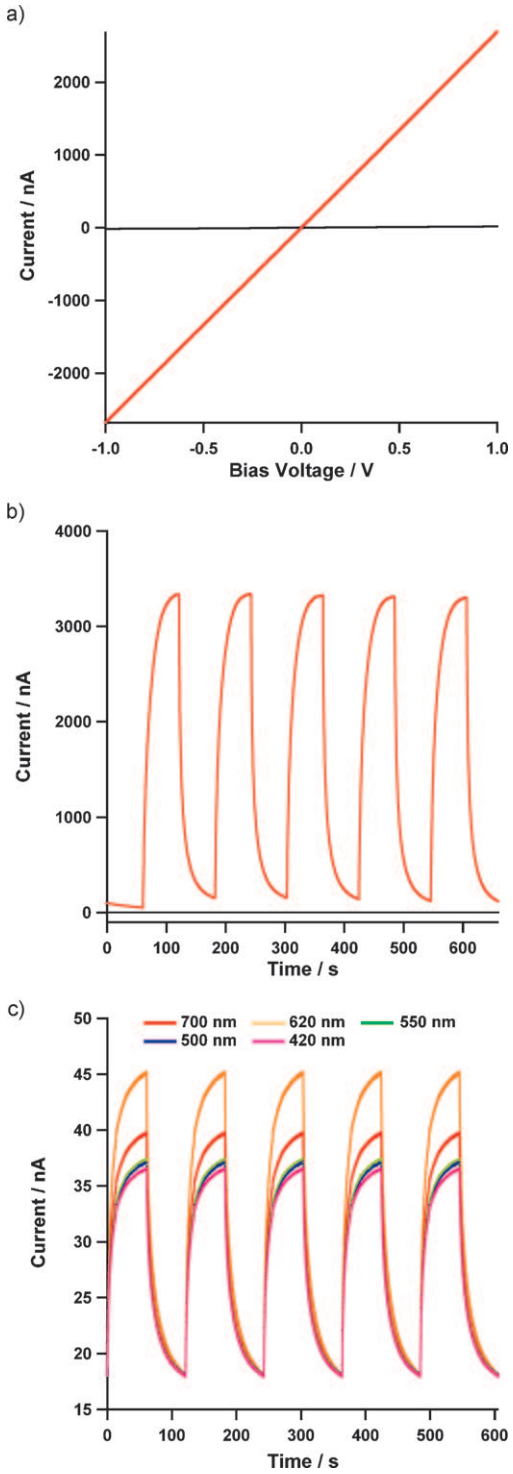

Figure 5. a) *I–V* curves in the dark (black curve) and upon irradiation (red curve) with a xenon light source. b) The photocurrent for NiPc COF (red curve) and [$(MeO)_8$PcNi] (black curve) at a bias voltage of 1.0 V, generated by repeatedly switching the light on and off. c) Wavelength-dependent on–off switching of photocurrent at a bias voltage of 1.0 V.

potential of two-dimensional covalent organic frameworks in novel optoelectronics applications.

Received: September 21, 2010
Published online: December 23, 2010

Keywords: carrier transport · covalent organic frameworks · photoconduction · phthalocyanines · porous materials

[1] a) A. P. Côté, A. I. Benin, N. W. Ockwig, M. O'Keeffe, A. J. Matzger, O. M. Yaghi, *Science* **2005**, *310*, 1166–1170; b) A. P. Côté, H. M. El-Kaderi, H. Furukawa, J. R. Hunt, O. M. Yaghi, *J. Am. Chem. Soc.* **2007**, *129*, 12914–12915; c) H. M. El-Kaderi, J. R. Hunt, J. L. Mendoza-Cortés, A. P. Côté, R. E. Taylor, M. O'Keeffe, O. M. Yaghi, *Science* **2007**, *316*, 268–272; d) S. S. Han, H. Furukawa, O. M. Yaghi, W. A. Goddard III, *J. Am. Chem. Soc.* **2008**, *130*, 11580–11581; e) J. R. Hunt, C. J. Doonan, J. D. LeVangie, A. P. Côté, O. M. Yaghi, *J. Am. Chem. Soc.* **2008**, *130*, 11872–11873; f) F. J. Uribe-Romo, J. R. Hunt, H. Furukawa, C. Klock, M. O'Keeffe, O. M. Yaghi, *J. Am. Chem. Soc.* **2009**, *131*, 4570–4571; g) H. Furukawa, O. M. Yaghi, *J. Am. Chem. Soc.* **2009**, *131*, 8875–8883; h) C. J. Doonan, D. J. Tranchemontagne, T. G. Glover, J. H. Hunt, O. M. Yaghi, *Nat. Chem.* **2010**, *2*, 235–238.

[2] a) R. W. Tilford, W. R. Gemmill, H. C. zur Loye, J. J. Lavigne, *Chem. Mater.* **2006**, *18*, 5296–5301; b) R. W. Tilford, S. J. Mugavero III, P. J. Pellechia, J. J. Lavigne, *Adv. Mater.* **2008**, *20*, 2741–2746.

[3] a) P. Kuhn, M. Antonietti, A. Thomas, *Angew. Chem.* **2008**, *120*, 3499–3502; *Angew. Chem. Int. Ed.* **2008**, *47*, 3450–3453; b) X. Wang, K. Maeda, A. Thomas, K. Takanabe, G. Xin, J. M. Carlsson, K. Domen, M. Antonietti, *Nat. Mater.* **2009**, *8*, 76–80; c) M. J. Bojdys, J. Jeromenok, A. Thomas, M. Antonietti, *Adv. Mater.* **2010**, *22*, 2202–2205.

[4] a) S. Wan, J. Guo, J. Kim, H. Ihee, D. Jiang, *Angew. Chem.* **2008**, *120*, 8958–8962; *Angew. Chem. Int. Ed.* **2008**, *47*, 8826–8830; b) S. Wan, J. Guo, J. Kim, H. Ihee, D. Jiang, *Angew. Chem.* **2009**, *121*, 5547–5550; *Angew. Chem. Int. Ed.* **2009**, *48*, 5439–5442.

[5] a) N. L. Campbell, R. Clowes, L. K. Ritchie, A. I. Cooper, *Chem. Mater.* **2009**, *21*, 204–206; b) T. Hasell, X. Wu, J. T. A. Jones, J. Bacsa, A. Steiner, T. Mitra, A. Trewin, D. J. Adams, A. I. Cooper, *Nat. Chem.* **2010**, *2*, 750–755.

[6] E. L. Spitler, W. R. Dichtel, *Nat. Chem.* **2010**, *2*, 672–677.

[7] C. H. Lee, R. Filler, J. Lee, J. Li, B. K. Mandal, *Renewable Energy* **2010**, *35*, 1592–1595.

[8] K. M. Kadish, K. M. Smith, R. Guilard, *The Porphyrin Handbook*, Vol. 15–20, Academic Press, **2002**.

[9] J. Piris, T. E. Dykstra, A. A. Bakulin, P. H. M. van Loosdrecht, W. Knulst, M. T. Trinh, J. M. Schins, L. D. A. Siebbeles, *J. Phys. Chem. C* **2009**, *113*, 14500–14506.

[10] L. Chen, Y. Honsho, S. Seki, D. Jiang, *J. Am. Chem. Soc.* **2010**, *132*, 6742–6748.

